Changes at the KinA PAS-A Dimerization Interface Influence Histidine Kinase Function[†,‡]

James Lee,[§,||] Diana R. Tomchick,[§] Chad A. Brautigam,[§] Mischa Machius,[§] Remco Kort,[⊥,#] Klaas J. Hellingwerf,[⊥] and Kevin H. Gardner*[,§,||]

Departments of Biochemistry, Pharmacology, UT Southwestern Medical Center, 5323 Harry Hines Blvd., Dallas, Texas 75390, and Molecular Microbial Physiology Group, Swammerdam Institute for Life Sciences, BioCentrum, University of Amsterdam, Nieuwe Achtergracht 166, 1018 WV Amsterdam, The Netherlands

Received October 20, 2007; Revised Manuscript Received February 6, 2008

ABSTRACT: The *Bacillus subtilis* KinA protein is a histidine protein kinase that controls the commitment of this organism to sporulate in response to nutrient deprivation and several other conditions. Prior studies indicated that the N-terminal Per-ARNT-Sim domain (PAS-A) plays a critical role in the catalytic activity of this enzyme, as demonstrated by the significant decrease of the autophosphorylation rate of a KinA protein lacking this domain. On the basis of the environmental sensing role played by PAS domains in a wide range of proteins, including other bacterial sensor kinases, it has been suggested that the PAS-A domain plays an important regulatory role in KinA function. We have investigated this potential by using a combination of biophysical and biochemical methods to examine PAS-A structure and function, both in isolation and within the intact protein. Here, we present the X-ray crystal structure of the KinA PAS-A domain, showing that it crystallizes as a homodimer using β-sheet/β-sheet packing interactions as observed for several other PAS domain complexes. Notably, we observed two dimers with tertiary and quaternary structure differences in the crystalline lattice, indicating significant structural flexibility in these domains. To confirm that KinA PAS-A also forms dimers in solution, we used a combination of NMR spectroscopy, gel filtration chromatography, and analytical ultracentrifugation, the results of which are all consistent with the crystallographic results. We experimentally tested the importance of several residues at the dimer interface using site-directed mutagenesis, finding changes in the PAS-A domain that significantly alter KinA enzymatic activity *in vitro* and *in vivo*. These results support the importance of PAS domains within KinA and other histidine kinases and suggest possible routes for natural or artificial regulation of kinase activity.

Bacteria sense and respond to a wide range of changes in the environment around them using two-component signaling systems (*1*). In their simplest form, these signaling pathways utilize two classes of proteins: histidine kinases and response regulators. The former serve as sensors that are activated in response to alterations in specific environmental parameters. The activation of these kinases leads to autophosphorylation of an essential histidine residue, followed by one or more subsequent phosphoryl transfer steps that culminate in the phosphorylation of an aspartate residue on the response regulator that alters its ability to regulate the transcription of target genes. Such two-component signaling pathways form the basis of a diverse set of bacterial signaling pathways, examples of which include those associated with *E. coli* chemotaxis (*2*), rhizobial oxygen responses (*3*), *Caulobacter* differentiation (*4*), and *Brucella* virulence (*5*).

Given this regulatory model, it is clear that control of histidine kinase activity is central to the regulation of two-component signaling systems. Many histidine kinases are composed of two functional regions: a catalytic domain that transfers a phosphoryl group from an ATP substrate to the conserved phosphoaccepting histidine residue and a sensory part that regulates kinase (and/or phosphatase) activity in response to environmental stimuli. Consistent with the diversity of signals that regulate these enzymes, sequence analyses show that the sensory regions of histidine kinases contain a wide variety of modular domains that are well-suited for the detection of various stimuli (*6*). These include Period-ARNT-Single-minded (PAS)[1] domains, which have been found in almost 2000 sensor kinases (*7*). PAS domains are found in a large group of proteins, ranging from enzymes to transcription factors to ion channels, in organisms in all three kingdoms of life (*8*). In spite of this diversity, these domains are structurally homologous. They share a mixed

[†] This work has been supported by grants from the NIH (GM-81875 to K.H.G.) and the NWO-STW (ABC-5587 to K.H. and R.K.).

[‡] Coordinates have been deposited with the RCSB PDB (PDB ID 2VLG).

* Corresponding author. Kevin H. Gardner, Department of Biochemistry, UT Southwestern Medical Center, 5323 Harry Hines Blvd., Dallas, TX 75390-8816. Phone: 1-214-645-6365. Fax: 1-214-645-6353. E-mail: Kevin.Gardner@utsouthwestern.edu.

[§] Department of Biochemistry, UT Southwestern Medical Center.

[||] Department of Pharmacology, UT Southwestern Medical Center.

[⊥] University of Amsterdam.

[#] Current address: TNO Quality of Life, Department of Microbiology, Utrechtseweg 48, 3704 HE Zeist, The Netherlands.

[1] Abbreviations: PAS domain, Period-ARNT-Single-minded (Per-ARNT-Sim) domain.

10.1021/bi7021156 CCC: $40.75
Published on Web 03/07/2008

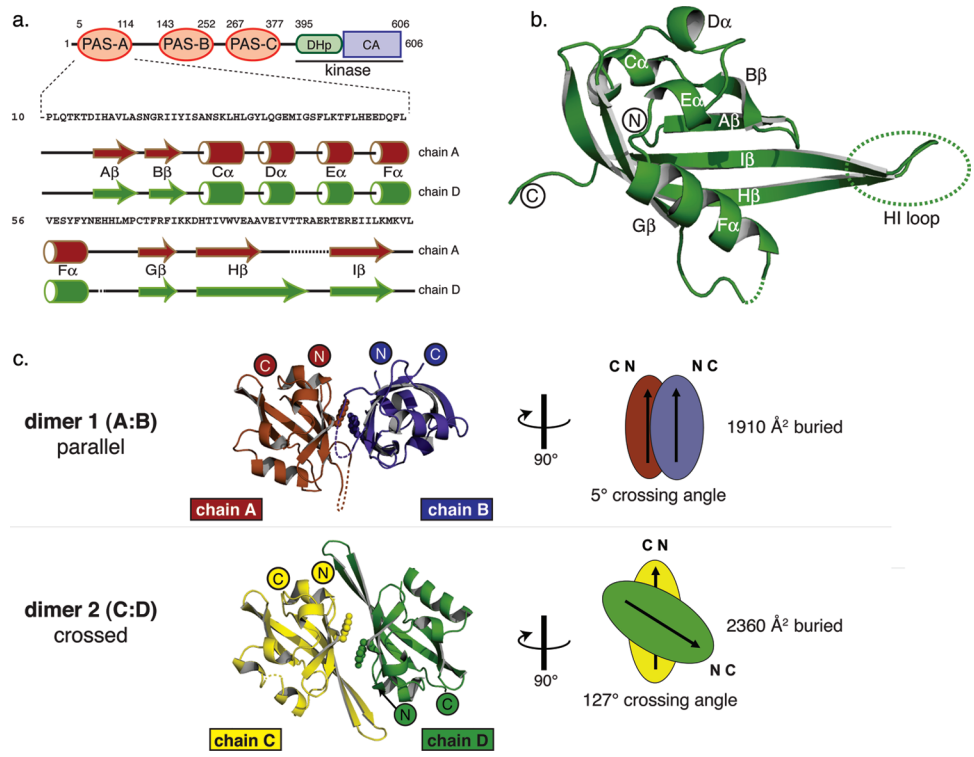

FIGURE 1: KinA architecture and PAS-A domain structure. (a) Schematic representations of KinA domain organization and PAS-A secondary structure. Approximate domain boundaries were obtained from Hidden Markov model analyses of the KinA sequence using the Pfam web service (*51*). The sequence of the construct used for our studies of the PAS-A domain is provided along with a ribbon representation of the secondary structure elements observed in the A and D monomers in the crystal structure. Dashed lines indicate regions that are disordered in these monomers (listed in Table 1). (b) Ribbon diagram of the D monomer of the KinA PAS-A crystal structure, labeled using the nomenclature established for PAS secondary structure elements by Gong et al. (*44*). The HI loop, which is disordered in the A and B monomers, is indicated with a dotted circle. (c) Ribbon diagrams of the two types of PAS-A dimers that were observed in the crystal structure, presented with monomers A and C in the same orientation. While both dimers use the same β-sheet interface, they differ in their buried surface areas and interstrand packing angles (determined by measuring the crossing angle of the Iβ strands). PAS-A structures shown in Figures 1 and 2 all use the same color scheme (chain A, brown; B, blue; C, yellow; D, green).

α/β fold of approximately 110 amino acid residues and typically interact with other protein sequences either in cis or in trans using an exposed face of a central β-sheet (*9*). Intriguingly, many PAS domains can themselves serve as sensors by binding environmentally sensitive cofactors that control the conformation of the surrounding protein domain and thus alter its ability to interact with protein targets (*10, 11*).

This model of PAS domain function suggests that such domains can play critical roles within sensory regions of histidine kinases. We have chosen to investigate this aspect by studying the *Bacillus subtilis* KinA kinase, the most important of several histidine kinases that regulate the initiation of sporulation in this organism (*12–14*). KinA is primarily responsible for controlling this response under laboratory conditions, as demonstrated by the significantly decreased sporulation efficiency of *kinA* strains (*14*). Upon initiation of sporulation by unknown signal(s) correlated with nutrient starvation, KinA activates a phosphorelay that ends with phosphorylation of the essential response regulator Spo0A and subsequent modulation of the expression of approximately 120 genes (*15*). While biochemical and biophysical studies of this phosphorelay have revealed many details of the signaling process (*16*), the regulation of KinA kinase activity has ironically remained somewhat mysterious. Examination of the KinA domain structure shows that it can be divided into both a regulatory and a catalytic segment, the former of which consists of three PAS domains in tandem (Figure 1a). Several lines of evidence strongly suggest that these PAS domains play a critical role in controlling KinA activity, particularly the observation that deletion of the N-terminal PAS-A domain reduces KinA autophosphorylation activity by approximately 95% (*17*).

To further explore this regulation, we have investigated the structure and function of the KinA PAS-A domain using a combination of biophysical and biochemical approaches. We start by presenting the X-ray crystal structure of the KinA PAS-A domain, showing that it adopts a dimeric conformation in the crystal using β-sheet/β-sheet packing interactions consistent with the behavior of several other PAS domain complexes. Notably, we observed two dimers with differences in tertiary and quaternary structures in the crystalline lattice, indicating some degree of structural flexiblity in these domains. To confirm that the KinA PAS-A domain also adopts a dimeric structure in solution, we used a combination of NMR spectroscopy, gel filtration chromatography and analytical ultracentrifugation, the results of which all support our crystallographic findings. We experimentally tested the importance of several residues at the dimer interface using site-directed mutagenesis and found changes in the PAS-A domain that significantly alter KinA enzymatic activity *in vitro* and *in vivo*. These results emphasize the importance of PAS domains for signal sensing within KinA and other histidine kinases and suggest possible natural or artificial routes to modulate kinase activity.

Table 1: Data Collection, Phasing, and Refinement Statistics for KinA PAS-A Structure[a]

	data collection		
crystal	native	SeMet[b] peak	SeMet[b] inflection
energy (eV)	12,661.23	12,659.57	12,657.79
resolution range (Å)	44.8 – 1.71 (1.74 – 1.71)	30.41 – 2.00 (2.03 – 2.00)	37.69 – 2.00 (2.03 – 2.00)
unique reflections	42,220	57,603	54,515
multiplicity	2.9	3.5	1.6
data completeness (%)	88.0 (56.2)	99.0 (99.2)	92.9 (69.4)
R_{merge} (%)[c]	4.1 (41.8)	6.0 (22.1)	4.7 (22.4)
I/σ(I)	24.9 (1.92)	17.7 (4.9)	13.8 (2.4)
Wilson B-value (Å^2)	24.8	25.2	26.4
	phase determination		
anomalous scatterer	selenium, 12 out of 12 possible sites		
figure of merit	0.323 (30–2.00 Å)		
	refinement statistics		
resolution range (Å)	44.8 – 1.71 (1.75 – 1.71)		
no. of reflections R_{work}/R_{free}	40,811/1,499 (1,758/77)		
data completeness (%)	87.9 (52.8)		
atoms (non-H protein/solvent/other)	3,241/296/12		
R_{work} (%)	19.8 (26.6)		
R_{free} (%)	24.3 (31.9)		
overall anisotropic scale factors[d]	−1.51, 2.99, −1.53, 0.00, −0.07, 0.00		
rmsd bond length (Å)	0.018		
rmsd bond angle (°)	1.76		
mean B-value (Å^2; protein/solvent/other)	28.3/37.8/46.7		
Ramachandran plot (%; favored/additional/disallowed)	98.1/1.9/0.0		
missing residues	Chain A: 15–96, 104–114; B: 15–97, 105–114; C: 15–116; D: 15–68, 71–114		

[a] Data for the outermost shell are given in parentheses. [b] Bijvoet-pairs were kept separate for data processing. [c] $R_{merge} = 100\ \Sigma_h\Sigma_i|I_{h,i} - \langle I_h\rangle|/\Sigma_h\Sigma_i I_{h,i}$, where the outer sum (h) is over the unique reflections, and the inner sum (i) is over the set of independent observations of each unique reflection. [d] As defined in REFMAC5 (*25*).

MATERIALS AND METHODS

Protein Expression and Purification: KinA PAS-A. The DNA encoding *Bacillus subtilis* KinA was PCR-amplified from chromosomal DNA isolated from *B. subtilis* strain 1A40 (Bacillus Genetic Stock Center, Columbus, OH) and cloned into the pHis$_6$Gβ1-parallel vector (*10*) using *Eco*RI and *Xho*I restriction sites. The resulting plasmid encodes residues 10–117 of KinA fused with an N-terminal His$_6$Gβ1-tag and a TEV protease site in the tag-protein linker. This construct was transformed into *E. coli* BL21(DE3), and protein expression was triggered by inducing with 0.5 mM IPTG for 16 h at 20 °C. To prepare samples for NMR experiments, cells were grown in M9 minimal media containing 1 g/L of $^{15}NH_4Cl$ for uniformly ^{15}N samples, further substituting unlabeled glucose with 3 g/L of $^{13}C_6$-glucose for uniformly $^{15}N/^{13}C$ labeled samples. Uniformly deuterated proteins were generated using the same protocol, except cells were grown in M9 minimal media made with 99.9% D_2O. For crystallographic studies involving selenomethionine-labeled protein, methionine auxotroph *E. coli* B834 cells were grown in M9 media containing an amino acid mixture (25 mg/L for each amino acid except methionine) and supplemented with selenomethionine (50 mg/L). After induction, cells were harvested by centrifugation, and the resulting cell pellets were resuspended in buffer containing 25 mM Tris (pH 7.5), 100 mM NaCl, and 20 mM imidazole. After lysing cells with a cell disruptor and centrifuging, the resulting supernatant was loaded onto a Ni^{2+}-NTA column (GE Healthcare), eluted using a linear 20–500 mM imidazole gradient, and subsequently exchanged into imidazole-free buffer. The resulting sample was incubated overnight with His$_6$-TEV protease, and both the His$_6$-TEV and liberated His$_6$Gβ1 tag were removed by a combination of Ni^{2+}-loaded NTA and gel filtration (Superdex 75, GE Healthcare) chromatography. Mass spectrometry analyses confirmed that KinA PAS-A purified in this manner contained the expected vector-derived N-terminal GEF tripeptide followed by residues 10–117 from the wild type KinA sequence. Point mutations in KinA PAS-A were prepared using the QuikChange site-directed mutagenesis kit (Stratagene), and proteins containing these mutations were expressed and purified using the protocol established for the wild type protein.

Crystallization and X-ray Diffraction Data Collection. Crystals of KinA PAS-A were grown at 20 °C using the hanging-drop vapor-diffusion method. Hanging drops were made by mixing 1 μL of 7 mg/mL protein solution (25 mM Tris (pH 8.0), 100 mM NaCl) with 1 μL well solution containing 13–15% (w/v) PEG 10,000, 0.1 M ammonium acetate, and 0.1 M bis-Tris (pH 5.5), as determined from the Hampton Research Index Screen 2 (Hampton Research) sparse matrix screen. Crystals of selenomethionine-labeled protein were obtained under similar conditions, except that the protein solution also contained 20 mM DTT. Crystals grew to typical final dimensions of 80 × 80 × 100 μM within four days. For cryoprotection, crystals were transferred in steps into reservoir solutions containing increasing concentrations of glycerol, to a final glycerol concentration of 25% (v/v), and then flash-cooled in liquid propane. Native and anomalous dispersion data were collected under cryogenic conditions (100 K) using the Advanced Photon Source 19BM and 19ID beamlines, respectively. Our crystals exhibited the symmetry of space group $P2_1$ with unit cell parameters of *a*

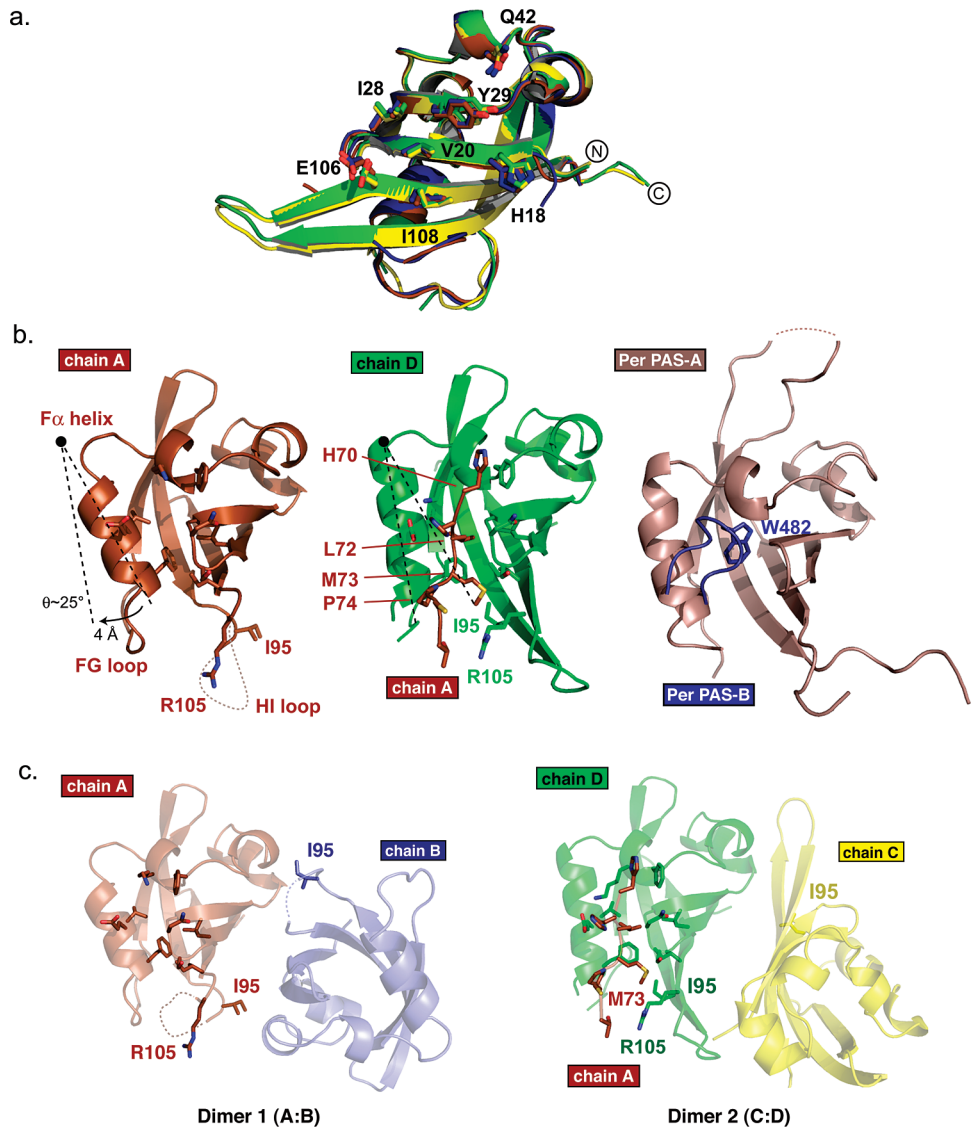

FIGURE 2: KinA PAS-A residues involved in dimer formation. (a) Side chain orientations at the dimer interface. A superimposition of all four monomers in the KinA PAS-A structure demonstrates that similar side chain orientations are found in residues at the center of the interface of the KinA PAS-A dimer. (b) Differences in tertiary and quaternary structure between the two dimeric forms as represented by diagrams of the structures of chain A (dimer 1) and chain D (dimer 2, with internally bound segment of chain A indicated). Also shown is the Per PAS-A structure that shares a similar intermolecular interaction with a loop from the PAS-B domain of another subunit (*48*), suggesting that other PAS-containing proteins use protein/protein interactions via regions similar to those in the KinA PAS-A dimer 2 structure. (c) Conformational differences of I95 in the two different dimeric arrangements. The I95 side chain is located at the β-sheet interface between monomers in the dimer 1 structure, but moves into the core of the monomers in the dimer 2 structure.

= 54 Å, b = 56 Å, c = 79 Å, and β = 109 degrees, contained four molecules of KinA PAS-A in the asymmetric unit with a solvent content of approximately 49%, and diffracted X-rays to a minimum Bragg spacing of about 1.7 Å. Diffraction was highly anisotropic leading to a significant decrease of the completeness at resolutions higher than about 2.0 Å. All data were processed using the HKL2000 suite of programs (*18*). Data collection statistics are provided in Table 1.

Phase Determination and Structure Refinement. Phases were obtained from a two-wavelength anomalous dispersion experiment using a seleno-methionine-KinA PAS-A crystal with data to a resolution of 2.0 Å. All 12 expected selenium sites were located using the program SHELXD (*19*). Phases were refined with the program MLPHARE (*20*), resulting in a figure-of-merit of 0.32. Phases were further improved by density modification and 4-fold noncrystallographic averaging with the program *DM* (*21*) resulting in a figure-of-merit of 0.75. An initial model containing about 80% of all residues was automatically generated using the program ARP/wARP (*22*). Additional residues were manually added using the program O (*23*). Refinement was carried out with native data to a resolution of 1.71 Å in the program CNS (*24*) and consisted of simulated annealing, conjugate-gradient minimization and refinement of individual B-factors, interspersed with manual revisions of the model. Refinement was completed with the program REFMAC5 (*25*) and included TLS refinement. The current model contains four KinA monomers (labeled A−D), which include residues 15–96 and 104–114 of chain A, residues 15–97 and 105–114 of chain B, residues 15–116 of chain C, and residues 15–68 and 71–114 of chain D, two acetate ions, four chloride ions, and 296 water molecules. The *R*-factor is 0.198, and the free *R*-factor is 0.243. A Ramachandran plot generated with Molprobity (*26*) indicated that 98.1% of all protein residues are in the most favored regions with the remaining 1.9% in

additionally allowed regions. All protein structure figures were generated using the program PyMOL (http://pymol.sf.net) in conjunction with the APBS plugin (*27*) for calculations of surface electrostatics. Calculations of buried surface areas used the Lee−Richards algorithm (*28*) as implemented in CNS. Model refinement statistics are provided in Table 1. Coordinates have been deposited with the RCSB PDB (PDB ID 2VLG). An assessment of the similarity of the KinA PAS-A structure to the canonical PAS domain fold was accomplished using the MultiProt web service (*29*), using chain D of the KinA PAS-A structure and six representative PAS domain structures (RCSB codes 1LL8, 1P97, 1X0O, 1BYW, 1G28, 1D06). From this ensemble, MultiProt automatically aligned all seven structures using a total of 59 Cα positions (KinA residues 17–21, 27–33, 35, 37–38, 40, 43, 45–54, 75–96 and 105–114), corresponding to almost all of the residues located in secondary structure elements in KinA PAS-A. The average Cα rmsd (at these 59 positions) of KinA PAS-A to the other six members of this group is 1.54 Å.

NMR Spectroscopy of KinA PAS-A. Backbone ^{15}N, ^{13}C, and ^{1}H chemical shift assignments of wild type and Y29A KinA PAS-A were generated from triple resonance NMR data recorded at 25 °C using a cryoprobe-equipped Varian Inova 600 MHz spectrometer. Assignments of wild type KinA PAS-A were obtained from a 800 μM sample of ^{15}N/^{13}C/^{2}H labeled protein in 25 mM Tris (pH 7.5), 100 mM NaCl, and 5 mM DTT, using data from a combination of ^{2}H-decoupling modified 3D HNCA, HN(CO)CA, HNCACB, HN(COCA)CB, and HNCO experiments (*30*) and a 3D ^{15}N-edited NOESY spectrum. For the Y29A mutant, a sample of 400 μM ^{15}N/^{13}C labeled protein in the same buffer was used to record 3D HNCACB, CBCA(CO)NH, HNCO (reviewed in ref *31*), and simultaneous ^{15}N,^{13}C-edited NOESY spectra (*32*). Two-dimensional ^{15}N/^{1}H HSQC spectra were recorded of these and other KinA PAS-A variants using standard sensitivity-enhanced pulse sequences (*33*). All NMR data were processed using nmrPipe (*34*) for data processing and analyzed with NMRview (*35*).

Analytical Ultracentrifugation and Gel Filtration Chromatography. Analytical ultracentrifugation experiments were conducted using a Beckman XL-I analytical ultracentrifuge. Sedimentation velocity analytical ultracentrifugation measurements were carried out using 12 mm charcoal-filled Epon double-sector cells with sample volumes of 400 μL. Concentrations were adjusted so that protein samples had absorbance readings at 280 nm (A_{280}) of 0.5 (equivalent to 44 μM monomer of wild type KinA PAS-A and all point mutants except Y29A; 50 μM for Y29A). To assess the concentration dependence of measured $s_{20,w}$ values for wild type KinA, Y29A, and I95E, additional data were collected at A_{280} values of 0.1, 0.4, and 0.9 (9, 36, and 81 μM for WT and I95E; 10, 40, and 90 μM for Y29A). Data were recorded at a speed of 50,000 rpm in an An-60Ti rotor at 25 °C using interference and absorbance optics. These data were analyzed using SedPHAT (*36*). Analytical gel filtration chromatography experiments utilized 1 mL samples of proteins at 200–300 μM concentrations (50 mM Tris at pH 7.5; 100 mM NaCl) injected onto a Superdex 75 column (GE Healthcare).

Protein Expression and Purification: KinA. Following the procedures described above for KinA PAS-A, constructs were generated for the full-length KinA protein (residues 1–606) and a version lacking the PAS-A domain (ΔPAS-A, residues 151–606), starting with PCR amplification of chromosomal DNA and cloning into the *Eco*RI and *Xho*I restriction sites of the pHis$_6$-parallel vector (*37*). Following protein overexpression and centrifugation, cells containing His$_6$-KinA proteins were resuspended in buffer containing 25 mM Tris (pH 8.0), 100 mM NaCl, 5 mM EDTA, and 5% (v/v) glycerol. After lysis, His$_6$-KinA was purified using the procedure described for KinA PAS-A, except that the gel filtration chromatography step was performed with a Superdex 200 column (GE Healthcare).

In Vitro Kinase Assays. Phosphorylation reactions were conducted as previously outlined by Wang et al. (*17*). In summary, reactions were carried out in 40 μL volumes of reaction buffer (25 mM Tris (pH 7.5), 100 mM NaCl, 0.1 mM EDTA, 20 mM $MgCl_2$, and 5% (v/v) glycerol) containing 4 μM KinA protein and 5 μCi (γ-^{32}P) ATP (3,000 Ci/mmol; DuPont-NEN) mixed with unlabeled ATP to give a final ATP concentration of 400 μM. Reactions were initiated by the addition of ATP, allowed to proceed at 25 °C for various times between 2 and 18 min (Figure 6B) or for a uniform 8 min duration (Figure 6C), and terminated by adding 5× SDS−PAGE sample buffer. Samples were analyzed using SDS−PAGE with 10% acrylamide gels that were electrophoresed at a constant voltage of 240 V for 35 min or until the dye front had migrated at least 75% of the gel length. After removing the lower portions of these gels containing the dye front with unincorporated ^{32}P-ATP, gels were dried at 80 °C under vacuum. Bands containing ^{32}P-phosphorylated proteins were visualized by exposing dried gels to Fujifilm phosphorimager screens for 16 h at room temperature and quantified using a Fujifilm FLA-5100 phosphorimager and the accompanying ImageQuant software (Molecular Dynamics).

Construction of Plasmids for in Vivo Analyses of KinA Function. Sequences for full-length and ΔPAS-A KinA (residues 1–606 and 151–606, respectively) were PCR-amplified and cloned into the pDG148 vector (Bacillus Genetic Stock Center, Columbus, OH) using *Hind*III and *Sph*I restriction sites to generate the pKinA and pKinAΔPAS-A plasmids. These plasmids, which express the inserted genes under the control of an IPTG inducible promoter, were then transformed into *B. subtilis* strain IIA-gfp (*38*). To overcome the problem of other kinases feeding signals into the phosphorelay, the KinA function is specifically addressed here by artificially overproducing KinA under nonsporulating growth conditions, which results in mechanistically similar sporulation activation, as previously described (*39*). The IIA-gfp strain also has the *gfp* gene placed under the control of the *spoIIA* promoter, providing a way to monitor KinA activity via the function of the entire sporulation phosphorelay as reconstituted in physiologically active cells (Supporting Information, Figure S3).

Colony Microscopy. Colonies of *B subtilis* were observed and photographed using a stereoscopic 0.8 to 8× zoom microscope SMZ-1000 (Nikon Corporation, Tokyo, Japan), equipped with two 10× oculars and a 0.5× objective (working distance, 123.6 mm). The microscope contained an epifluorescence attachment and a Nikon DXM-1200 digital camera system. The EclipseNet software package version 1.16.2 was used for control of the camera settings

and image processing. Fluorescent *B. subtilis* reporter strains were monitored by the use of an HBO 103W/2 mercury short arc lamp (Osram Inc.) and a long pass GFP filter (excitation 460–500 nm, DM505, BA510). All fluorescence pictures were taken with a 1 s exposure time and default color balance settings (gain settings: red, 30; green, 10; blue, 50) and processed identically.

Flow Cytometry Analysis. Transformed *B. subtilis* cells harboring various constructs were first propagated overnight in liquid cultures in LB media containing 10 μg/mL kanamycin and 5 μg/mL chloramphenicol and then rediluted to $OD_{600} = 0.1$ in the same medium supplemented with 25 μM IPTG and grown under aerobic conditions for 4 h. Subsequently, cells were diluted 40-fold in 0.2 μM-filtered Isoton II media (Beckman Coulter) and directly measured on a Coulter Epics XL-MCL flow cytometer (Beckman Coulter) equipped with an argon ion laser (488 nm). For each sample, at least 10,000 cells were analyzed. The GFP signals were collected using a fluorescein isothiocyanate filter, with the photomultiplier voltage set to 800 V. Data were captured using Expo32 ADC cytometry list mode data acquisition and analysis software version 1.1.C (Beckman Coulter) and further analyzed using Origin version 7 (OriginLab Corporation, Northampton, MA, USA). Histogram curves describing the number of events versus fluorescence intensity were fitted with Gaussian curves. Each fit had a determination coefficient $R^2 \geq 0.9$ and was used to extract a maximum position, referred to as its Mxc value.

RESULTS

Crystal Structure of the KinA PAS-A Domain. The crystal structure of KinA PAS-A (residues 10–117) was determined using the selenomethionyl MAD phasing method (*40*) and refined against data to a resolution of 1.71 Å. The asymmetric unit of our crystals contains four KinA PAS-A molecules, designated as monomers A–D. Overall, the structures of all four molecules are very similar, with residues 17–113 adopting a typical mixed α/β fold found in other PAS domains (Figure 1a and b). The most notable differences occur in the A and B monomers, both of which have seven disordered residues in the HI loops that connect the Hβ and Iβ strands (Figure 1a and b), whereas these loops are fully ordered in molecules C and D. Structure-based alignment (*29*) of the KinA PAS-A structure to six other PAS domain structures solved by X-ray crystallography or NMR spectroscopy shows an average pairwise Cα rmsd (between KinA PAS-A and the other six proteins) of 1.54 Å for 59 Cα positions in secondary structure elements, establishing that our structure is very similar to the standard PAS domain fold. In contrast to structures of several ligand-binding PAS domains (e.g., FixL (*41*)), KinA PAS-A does not contain any internally bound cofactors or any preformed pockets that could potentially accommodate the binding of such compounds.

The four KinA PAS-A monomers in the asymmetric unit arrange into two distinct types of dimers, composed of monomers A and B (dimer 1), and monomers C and D (dimer 2), respectively (Figure 1c). The structures of the monomers within the dimers are very similar with rmsd values of 0.3 Å for dimer 1 and dimer 2 (for 59 equivalent Cα atoms in regular secondary structure elements), whereas monomers from different dimers show slightly higher rmsd values (between 1.0 and 1.1 Å for the same 59 Cα atoms). Both dimers employ the same β-sheet interface used by a diverse collection of PAS domains to form both intramolecular (*10, 42, 43*) and intermolecular interactions (*9, 44–46*), including homo and heterodimerization of PAS domains. Despite this similarity, the two dimers differ in their relative intersubunit orientation, with dimer 1 assuming an almost parallel orientation ($\sim$5° crossing angle), while dimer 2 orients the two domains such that they cross each other with a $\sim$120° angle. These two packing arrangements lead to significantly different buried surface areas: 1,910 Å^2 for dimer 1 versus 2,360 Å for dimer 2. Part of this difference is due to the HI loops, which are disordered in monomers A and B but participate in dimer formation between monomers C and D.

The two orientations within the KinA PAS-A dimers are related by a rotation about a central axis in the β-sheet near Y29. This residue interacts with the analogous Y29 residue on the adjacent dimerization partner (Figure 1c) and is joined by H18, V20, I28, Q44, E106, and V108 to form a chiefly hydrophobic interface between the two monomers. Most of these residues belong to the central β-sheet (except Q44, which is located in the Dα helix) and adopt similar side chain orientations in all four monomers (Figure 2a). This observation suggests that these residues form a stable interaction surface that is compatible with the formation of both types of dimers despite the significantly different monomer/monomer orientations that we observed. We note that the lattice contacts for each of the two types of dimers appear to be equivalent and limited in their extent, with the exception of an interaction involving the FG loops of dimer 1 subunits (discussed below).

Further examination of the two dimers reveals a novel intermolecular interaction that appears to correlate with the different monomer orientations in the two types of dimers. Notably, while the two dimer 1 monomers (A and B) adopt compact structures, both of the dimer 2 monomers (C and D) are slightly expanded. This expansion is due to a $\sim$25° rotation of the Fα helix about an axis near its N-terminus, moving it away from the rest of the domain. This rotation results in a 4 Å displacement of the C-terminus of the Fα helix and the formation of a cleft between this helix and the Eα helix and other parts of the domain. This cleft is partially occupied by a five-residue segment (H70−P74) of the FG loop from a monomer in an adjacent dimer 1. This interaction buries a significant amount of surface area (915 Å^2) and involves the hydrophobic side chains of both proteins. One set of these FG loop interactions occurs between dimers in the same asymmetric unit, but a second set occurs across a unit cell interface and may stabilize the crystalline lattice. Intriguingly, the cleft that accommodates FG loop binding is analogous to the regions where several other PAS domains bind their native ligands (e.g., FMN within phototropin (*47*)) or to the regions of other PAS domains that stabilize protein/protein complexes (e.g., *Drosophila* period (*48*); Figure 2b).

The rotation of the Fα helix also causes significant changes in the backbone conformation of the C-terminus of the Hβ strand, most notably near I95. In the dimer 1 monomers, this residue is located on the external surface of a β-bulge, allowing it to participate in monomer/monomer interactions (Figure 2c). In contrast, dimer 2 has significantly different backbone conformations for residues E93−I95, which no longer adopt a β-bulge conformation. This structural change

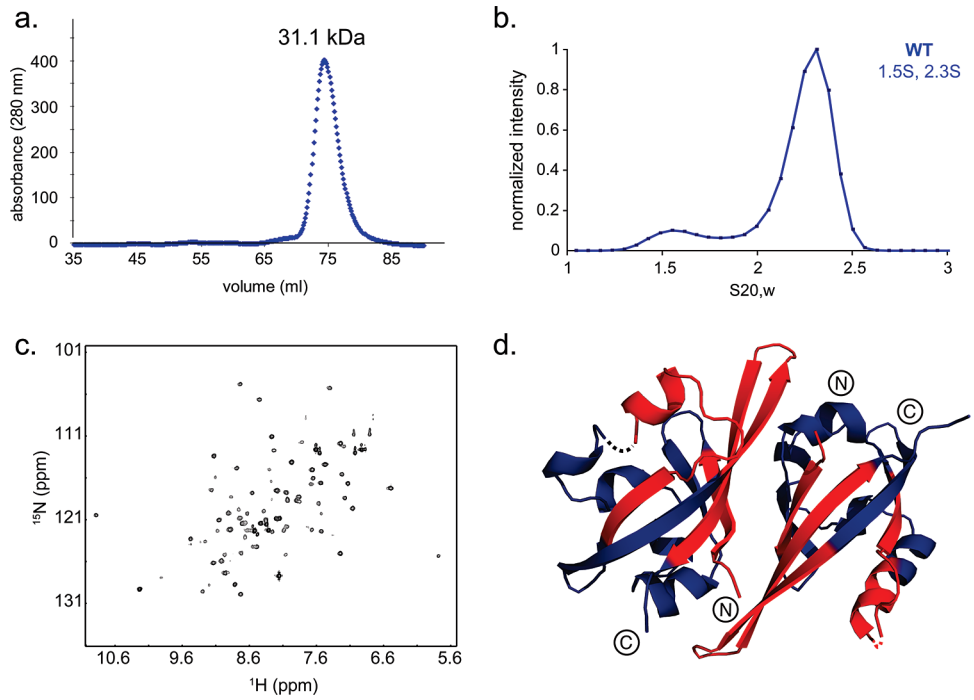

FIGURE 3: Dimerization properties of KinA PAS-A. (a) Gel filtration chromatography elution profile, indicating that the PAS-A domain has a hydrodynamic radius corresponding to that of a spherical particle with a 31 kDa molecular weight, consistent with the 26 kDa molecular weight of a dimer calculated from the KinA PAS-A sequence. (b) Analysis of sedimentation velocity profiles of KinA PAS-A (36 μM concentration). Two independent or slowly interconverting species exist in solution with $s_{20,w}$-values 1.5 and 2.3 S. As noted in the text, we attribute the more rapidly sedimenting species to a stable homodimer and the more slowly sedimenting species to a small amount of noninteracting monomers as indicated by the fact that the ratio of these two species is independent of protein concentration. (c) ^{15}N/^{1}H HSQC spectrum of KinA PAS-A. A significant number of the expected cross-peaks exhibit significant heterogeneity in peak intensity or are completely missing (sections of this spectrum are shown in detail in Supporting Information, Figure S2). (d) Residues with solution NMR chemical shift assignments from ^{2}H/^{13}C/^{15}N-labeled samples of KinA PAS-A (blue) are mapped onto the dimer 2 structure, demonstrating that most of the residues with significant broadening in ^{15}N/^{1}H HSQC spectra (c) are located at the dimeric interface, consistent with intermediate exchange broadening at those sites.

Table 2: Summary of Biophysical and Biochemical Properties of KinA

	isolated KinA PAS-A domain				full length KinA	
construct	S75 elution volume	S75 calculated MW[a]	dissociation constant[b]	species observed in sedimentation velocity[c]	*in vitro* activity (specific activities)[d]	*in vivo* activity (Mxc values)[e]
WT	74.2 mL	31.1 kDa	<9 μM (V)	2.3 S*, 1.5 S	2.3 ± 0.8	475
I95E	77.3 mL	25.7 kDa	95 μM (V)	1.5 S, 2.2 S	0.8 ± 0.2	450 (−15%)
I95A	78.6 mL	23.9 kDa	not determined	1.4 S, 2.1 S	1.3 ± 0.6	481 (+4%)
I108A	81.2 mL	20.5 kDa	not determined	1.7 S	2.8 ± 0.8	490 (+9%)
Y29A	85.2 mL	16.1 kDa	>300 μM (V,N)	1.5 S	4.0 ± 0.6	570 (+56%)
ΔPAS-A	not applicable	not applicable	not applicable	not applicable	~0.2#	376 (−56%)
no KinA expressed	not applicable	not applicable	not applicable	not applicable	not applicable	304

[a] Estimate of molecular weight based on the assumption of an ideal spherical particle and prior column calibrations. [b] K_d values (or estimates) are provided for each construct along with the source: V = ultracentrifugation sedimentation velocity, and N = solution NMR ^{15}N relaxation measurements of rotational correlation times. [c] Two species were observed for WT, I95E, and I95A in these data. For WT, the 2.3 S species was predominant and designated with an asterisk (*). For I95E and I95A, we observed concentration-dependent amounts of two species, which were roughly equally populated at 36 μM and shifted toward a predominant 2.1 or 2.2 S species within increasing protein concentration. [d] Units for our *in vitro* kinase assay: pmol ^{32}P·(nmol kinase)$^{-1}$·min^{-1}. As we were unable to observe significant autophosphorylation activity for the ΔPAS-A construct using our *in vitro* assay system, we here report an estimate (designated with an #) calculated by multiplying the specific activity of our WT KinA construct by the 92% reduction in initial autophosphorylation activity of an MBP-KinA(143–606) fusion (compared to an MBP-KinA control) reported by Wang et al. (*17*). [e] Mxc values: maximum of Gaussian distribution of fluorescence intensities. Percentage changes from wild type activity are shown in parentheses and calculated by % change = $100*[1-(\mathrm{Mxc}_{\mathrm{mutant}} - \mathrm{Mxc}_{\mathrm{no\ KinA}})/(\mathrm{Mxc}_{\mathrm{WT}} - \mathrm{Mxc}_{\mathrm{no\ KinA}})]$.

removes I95 from the surface, allowing it to interact with the M73 residue located on the FG loop provided by a neighboring dimer 1.

Solution Studies of PAS-A Dimerization. To investigate whether KinA PAS-A could form dimers in solution analogous to those observed in our crystal structure, we used a combination of gel filtration chromatography, analytical ultracentrifugation, and NMR spectroscopy. Superdex 75 gel filtration chromatography provided our first evidence of the formation of stable KinA PAS-A dimer under these conditions, as indicated by a hydrodynamic radius consistent with a spherical 31.1 kDa particle (Figure 3a; data also summarized in Table 2), which is only slightly larger than the 26.2 kDa size expected for a dimer.

This finding was supported by data from analytical ultracentrifugation analyses. Sedimentation velocity experiments indicate that KinA PAS-A exists in two independent or slowly interconverting species (Figure 3b). The majority of the protein exists as a 2.3 S species, which is consistent with a dimeric structure of the KinA PAS-A fragment as

indicated by the 24.3 kDa mass that can be calculated from this sedimentation coefficient in combination with the fitted value of the frictional ratio. In addition, HYDROPRO calculations (*49*) using our crystal structure coordinates predicted that a KinA PAS-A dimer should have a 2.1 S sedimentation coefficient, close to the observed value of 2.3 S. A minor fraction is present in a smaller 1.5 S form, the relative abundance of which remained low and constant over a concentration range of OD_{280} = 0.1–0.9 (9–81 μM monomer; data not shown). These data suggest that the bulk of KinA PAS-A exists as a stable dimer whose K_d is significantly below the lowest concentration tested (9 μM), while a small fraction exists as a minor species that cannot dimerize. These experiments provided no evidence supporting the existence of stable, higher molecular weight complexes in solution that could potentially be formed from the dimer/dimer interactions observed in our crystal structure.

Solution NMR spectroscopy provided additional data establishing that KinA PAS-A adopted a stable homodimer in solution. Two-dimensional $^{15}N/^{1}H$ HSQC spectra of ^{15}N-labeled samples revealed 72 of the 108 cross-peaks expected from the primary sequence. These cross-peaks had excellent ^{1}H chemical shift dispersion, confirming that the protein was well folded in solution (Figure 3c). Analyses of ^{15}N T_1 and T_2 relaxation rates from these samples indicated that KinA PAS-A had a 12.4 ns rotational correlation time at 25 °C, consistent with a 26 kDa homodimer complex (*50*). Adding residues onto the termini of the 10–117 construct (up to a maximum of residues 1–151) did not alter the dimerization behavior of the proteins as shown by gel filtration chromatography. (Data for a construct of residues 1–138 are provided in Supporting Information, Figure S1.) Furthermore, $^{15}N/^{1}H$ HSQC spectra of these larger fragments showed that additional sequences outside of residues 10–117 only generated signals with poor amide proton chemical shift dispersion, strongly suggesting that these new segments are disordered (data not shown).

Notably, our $^{15}N-^{1}H$ correlation spectra of the original construct (residues 10–117) showed significant heterogeneity in cross-peak linewidths and were missing a significant number of peaks (roughly 36 of the 108 cross-peaks expected from the primary sequence of the protein). This peak broadening was constant over a 50 μM to 1 mM range of KinA PAS-A concentrations, well above the K_d < 9 μM indicated by our ultracentrifugation studies (see above). This observation suggests that peak broadening might arise from intermediate time scale chemical-exchange broadening within a stable dimer. To identify the sites undergoing such exchange broadening, we generated uniformly $^{15}N,^{13}C,^{2}H$ labeled KinA PAS-A samples and used standard ^{2}H-decoupled triple resonance methods (*30*) to assign the backbone chemical shifts. Using these data, we were able to assign the backbone chemical shifts of roughly 50% of the residues, restricted almost entirely to residues on the α-helical surface located opposite to the dimer interface on the β-sheet (Figure 3d). Correspondingly, the missing cross-peaks appear to originate from significantly broadened sites in the β-sheet. These findings are consistent with KinA PAS-A being a stable dimer that might interconvert between multiple states, perhaps analogous to those observed in our crystal structure.

Structural Effects of Mutations at the PAS-A Dimerization Interface. To probe the functional importance of the dimerization interfaces identified by X-ray crystallography and our solution studies, we designed point mutations intended to disrupt these interfaces in KinA PAS-A. At the center of the β-sheet interface, Y29 and I108 were individually mutated to alanine to destabilize both types of dimer. Additionally, we changed I95 to either alanine or glutamic acid to investigate the role of this residue given its flip from the outside of the protein (dimer 1) into the core (dimer 2).

As assessed by several solution approaches, both the I108A and Y29A point mutations interfered with KinA PAS-A dimerization. Gel filtration chromatography of 200 μM protein samples showed both mutants apparently had smaller hydrodynamic radii than the wild type (Figure 4a). These hydrodynamic radii corresponded to molecular weights of ideal spherical particles of 20.5 kDa (I108A) and 16.1 kDa (Y29A), the latter of which is approximately half of that observed for the dimeric wild type KinA PAS-A. Turning to solution NMR, we found that the I108A $^{15}N/^{1}H$ HSQC spectrum had peak broadening similar to that of the wild type, suggesting that the protein was still dimeric at the tested concentration (800 μM). However, the Y29A mutant did not show the differential broadening observed in the wild type spectrum and instead had the expected number of cross-peaks with more uniform linewidths (Figure 4b and Supporting Information, Figure S2). Subsequent analysis of ^{15}N T_1 and T_2 relaxation rates established that the Y29A PAS-A construct had rotational correlation times of 8.4 ns (300 μM protein concentration), consistent with a monomeric protein. At higher concentrations, we observed an increase in rotational correlation time (11.6 ns at 1 mM protein), consistent with the monomer/dimer equilibrium being shifted to a K_d value exceeding 300 μM. Backbone chemical shift assignment of a $U^{-15}N/^{13}C$ labeled Y29A NMR sample established that this protein retained all of the regular secondary structural elements observed in the crystal structure (data not shown). Thus, we conclude from gel filtration data that the I108A mutation weakened the PAS-A dimer, whereas gel filtration and NMR results indicated that the Y29A mutation abolished dimer formation. Notably, both mutants retained the proper tertiary structure of the wild type protein.

To further investigate the nature of dimerization in KinA PAS-A, sedimentation velocity experiments were performed. These experiments indicated that both mutants were chiefly monomeric at OD_{280} = 0.5 (44 μM for I108A, 50 μM for Y29A), showing an average sedimentation coefficient of 1.6 S (Figure 4a), which is consistent with the calculated (*49*) hydrodynamic properties of a monomer taken from the KinA PAS-A dimers observed in our crystal structures. Additional experiments showed that the sedimentation behavior of the Y29A point mutant was invariant up to a maximum concentration of OD_{280} = 0.9 (90 μM). This observation is consistent with our NMR data showing that the Y29A point mutant has a K_d > 300 μM for the monomer/dimer equilibrium, representing a greater-than 30-fold increase over the K_d for dimerization of the wild type PAS-A domain.

The I95A and I95E point mutations were made with the intention to disrupt contacts flanking the central β-sheet dimerization interface that were only seen in the parallel dimer 1 conformation. Incorporation of either mutation into KinA PAS-A markedly changed the gel filtration elution

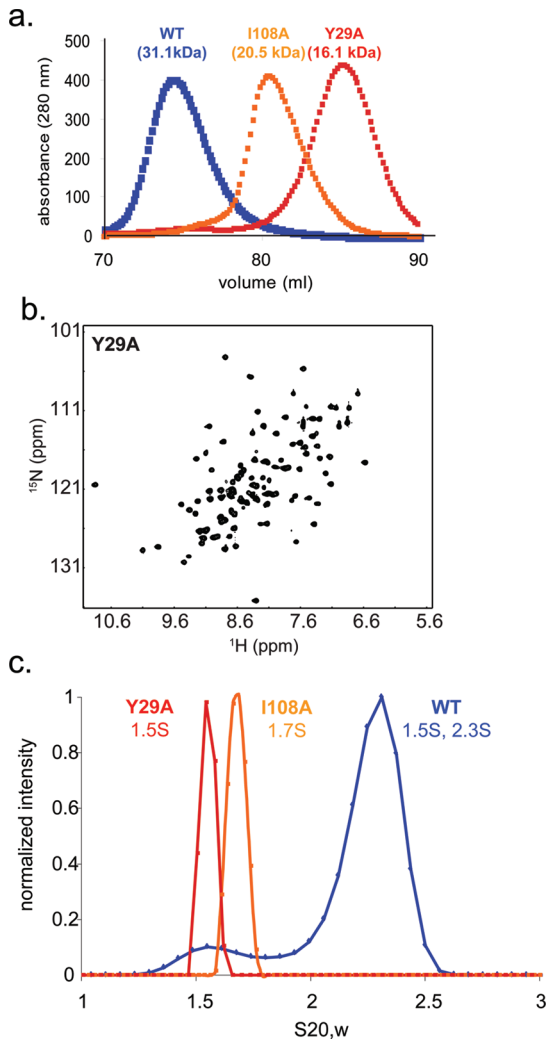

FIGURE 4: Analyses of the effects of the Y29A and I108A point mutations at the core of the KinA PAS-A β-sheet interface. (a) Gel filtration chromatography elution profiles for wild type, Y29A, and I108A PAS-A constructs. The elution profiles for the two point mutants are shifted towards smaller hydrodynamic radii, suggesting that these samples contain increased proportions of monomeric forms of each protein. (b) ^{15}N^{-1}H HSQC spectrum of Y29A mutant of PAS-A. Note the lack of differential broadening seen in spectra of the wild type KinA PAS-A. Detailed comparisons of spectra recorded on samples of the wild type and Y29A mutant proteins are provided in Supporting Information, Figure S2. (c) Sedimentation velocity profiles for Y29A and I108A (50 μM for Y29A; 44 μM for I108A) point mutants are compared with that of the wild type PAS-A domain (36 μM). These data indicate that both Y29A and I108A are present as single species with sedimentation coefficients of 1.5 and 1.7 S, respectively, consistent with a significant (I108A) or complete (Y29A) conversion to monomeric forms.

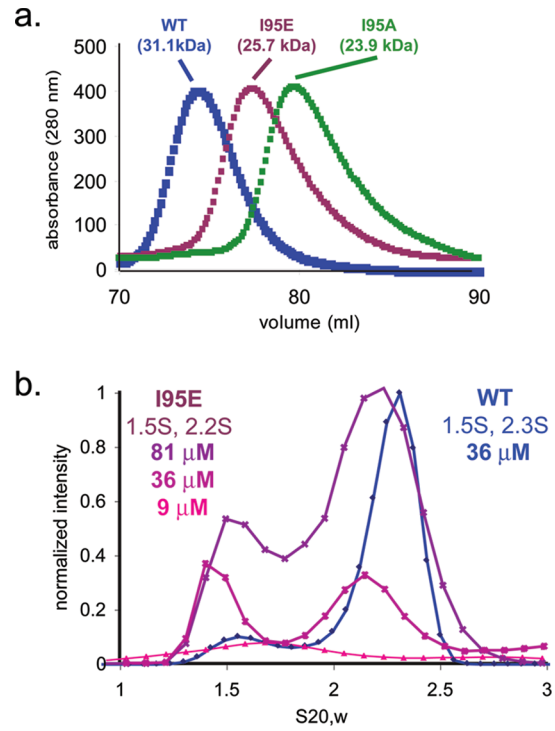

FIGURE 5: Analyses of the effects of I95A and I95E point mutations at the edge of the KinA PAS-A β-sheet interface. (a) Gel filtration elution profiles for wild type, I95A, and I95E PAS-A constructs. The elution profiles for both point mutants are shifted to longer elution volumes, suggesting a bias towards the monomeric form and/or changes in the shape of the dimer. (b) Sedimentation velocity profiles for the KinA PAS-A domain containing the I95E point mutant at three concentration values (9, 36, and 81 μM in pink, magenta, and purple) are compared with that of the wild type domain (36 μM in blue). The profiles for I95E are consistent with a slowly interconverting monomer/dimer mixture with a 95 μM dissociation constant, suggesting that the mutant protein is less efficient at dimer formation than the wild type protein.

profile as compared to that of the wild type protein (Figure 5a). The elution volumes were between those predicted for monomeric and dimeric KinA PAS-A, suggesting that the two I95 point mutants were either rapidly interconverting between monomers and dimers during the chromatography experiments or that they were monomeric and had undergone significant conformational changes compared to the wild type. To resolve this issue, we recorded ^{15}N$-^{1}$H HSQC spectra of both the I95E and I95A point mutants. These spectra had the same patterns of chemical shifts as wild type KinA PAS-A (data not shown), suggesting a change in dimerization equilibrium of these mutants, rather than a conversion into a monomer with drastically changed overall structure.

These conclusions are supported by sedimentation velocity ultracentrifugation data. As with wild type KinA PAS-A, two distinct peaks were observed at 1.5 S (monomer) and 2.2 S (dimer) in the velocity sedimentation profiles of the I95A and I95E mutants (Figure 5b). However, both mutants exhibited different population distributions for the monomeric and dimeric forms compared to the wild type. We further characterized this behavior with the I95E point mutant, which exhibited a significant concentration dependence of the monomer/dimer population distribution in the concentration range between 9 and 81 μM. Specifically, the amount of dimer increased with increasing protein concentration (Figure 5b). Results from the 9 and 81 μM samples were globally analyzed. The data were fitted using a kinetic Lamm equation model that explicitly takes into account the reaction kinetics for a monomer/dimer equilibrium. The quality of the fit was excellent; local rmsd values were 0.005 and 0.007 AU for the 9 and 81 μM samples, respectively. This analysis yielded a K_d of 95 μM and a slow off-rate ($k_{off} \sim 10^{-3}$ s^{-1}).

Mutations at the PAS-A Dimerization Interface Can Modulate Kinase Activity. To determine the importance of the PAS-A dimer interface for KinA function, we purified samples of full-length KinA containing the point mutations

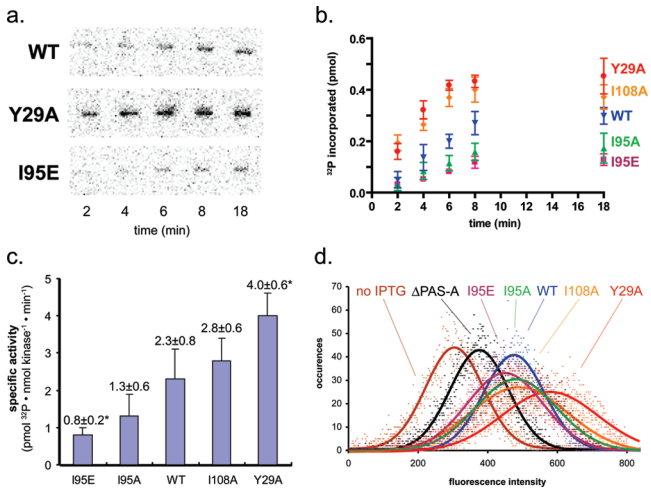

FIGURE 6: *In vitro* and *in vivo* functional assays of full-length KinA proteins. (a) *In vitro* autophosphorylation assays. Representative gels of ^{32}P incorporation for wild type KinA and the Y29A and I95E point mutants after incubation with γ^{32}P-ATP at indicated time points reveal that mutants exhibit enhanced or reduced kinase activity. Reactions were quenched at the indicated times and subjected to SDS−PAGE for quantitation of ^{32}P incorporation by phosphorimaging. (b) Progress of ^{32}P incorporation versus time for wild type and mutant constructs of KinA, as determined from *in vitro* kinase assays at a single 8 min fixed time point. Experiments were conducted in triplicate ($n = 3$). (c) Specific activities of wild type and mutant constructs ($n = 3$). Asterisks indicate statistically significant differences ($P < 0.05$) from wild type levels as determined by an unpaired Student's *t*-test. (d) *In vivo* assays of KinA function, provided by FACS analyses of GFP expression in *B. subtilis* strain IIA-gfp overexpressing KinA PAS-A, ΔPAS-A, and site-directed mutant constructs, showing that these mutants differentially modulate KinA activity. Lines indicate Gaussian fits to the raw profiles of distributions from FACS counting.

described above and assayed them for *in vitro* kinase activity. To characterize KinA autophosphorylation, we used a γ-^{32}P-ATP-based kinase assay and monitored ^{32}P incorporation as a function of time (Figure 6a and b). We observed that the PAS-A mutations either enhanced or inhibited autophosphorylation, with two of the mutations (Y29A and I95E) causing significant changes in kinase activity when incorporated into the full-length KinA protein. To quantify these differences, we determined specific activities from the time-dependence of ^{32}P incorporation over the first eight minutes of the assay (Figure 6c; data summarized in Table 2). The Y29A mutant KinA was significantly more active than wild type KinA, with a specific activity of 4.0 ± 0.6 pmol ATP•(nmol kinase)$^{-1}$•min^{-1} versus 2.3 ± 0.8 pmol ATP•(nmol kinase)$^{-1}$•min^{-1}. The I95A and I108A mutants of KinA had essentially the same kinase activity as that of the wild-type protein, with specific activities of 1.3 ± 0.6 and 2.8 ± 0.8 pmol ATP•(nmol kinase)$^{-1}$•min^{-1}, respectively. However, the I95E mutant of KinA displayed a statistically significantly lower specific activity than that of wild type: 0.8 ± 0.2 pmol ATP•(nmol kinase)$^{-1}$•min^{-1}. These results correlate with the sedimentation velocity data previously obtained from KinA PAS-A domains containing these same point mutations (see above): Y29A, an activating mutation in full-length KinA, shifts the PAS-A monomer/dimer equilibrium significantly toward the monomeric form (Figure 4). By contrast, the I95E mutant, with lowered KinA activity, retains significant PAS-A dimer content as shown by both gel filtration and sedimentation velocity measurements. These data suggest that activity of the full length KinA enzyme is linked to the oligomeric state adopted by the isolated PAS-A domain, but we note that we cannot formally rule out a direct involvement of I95 in the catalytic process.

To establish if these *in vitro* differences are also observed in the physiologically relevant context of the intact sporulation activation pathway *in vivo*, we evaluated these KinA mutants in an *in vivo* GFP-reporter assay of sporulation pathway activation. This assay is based on the introduction of full-length *kinA* genes (wild type or mutant) under the control of an IPTG-inducible promoter in the *B. subtilis* IIA-gfp strain (*38*), which places sporulation pathway activation under the specific control of overexpressed KinA activity. The transformed IIA-gfp strains express GFP under the control of the promoter of the *spoIIA* operon (whose expression is enhanced by Spo0A ~ P), facilitating the high-sensitivity observation of phosphorelay activation (Supporting Information, Figure S3a) in either intact colonies or in liquid cultures. Intact *B. subtilis* IIA-gfp colonies showed the expected dependence of GFP expression on KinA activity and demonstrated the requirement for an intact PAS-A domain at the N-terminus of KinA (Supporting Information, Figure S3b). Also, similar to the *in vitro* experiments described above, the Y29A point mutation activated KinA *in vivo* as shown by the enhanced GFP expression in colonies producing Y29A KinA (Supporting Information, Figure S3c).

For a more detailed analysis, we analyzed liquid cultures by measuring the fluorescence intensities of populations of *B. subtilis* IIA-gfp cells using fluorescence activated cell sorting (FACS). For each experiment, we measured the fluorescence of over 10,000 individual cells and fitted the profiles of these measurements to Gaussian distributions. For cells that did not express any KinA, the center of the (auto)fluorescence intensity distribution, designated as Mxc, was 304 (Figure 6d; data summarized in Table 2). Upon induction of wild type KinA with 100 μM IPTG, Mxc increased to 475. Cells expressing ΔPAS-A KinA had a smaller increase in fluorescence intensity (Mxc = 376; down 56% from wild type after subtracting background), consistent with the lower activity of the ΔPAS-A KinA enzyme observed *in vitro* (*17*). These experiments established a critical correlation between the *in vitro* and *in vivo* activities for the deletion mutant.

We then investigated the effects of our various site-directed mutants in the same manner. The Y29A mutant displayed the highest Mxc value of 570 (+56% from wild type), while I95E had the lowest Mxc value at 450 (−15%), consistent with our *in vitro* kinase assays (Figure 6d). In contrast, I95A and I108A displayed intermediate Mxc values of 481 (+4%) and 490 (+9%), respectively, that is, near the wild type level. Taken together, we conclude that changes at the KinA PAS-A dimerization interface generate functional consequences within the full-length KinA enzyme both *in vitro* and *in vivo*, that is, within the context of the sporulation activation pathway.

DISCUSSION

Using a combination of biophysical and biochemical approaches, we have characterized the structure and function of the PAS-A domain from *B. subtilis* KinA. In isolation, residues 17–113 (of a larger construct containing residues

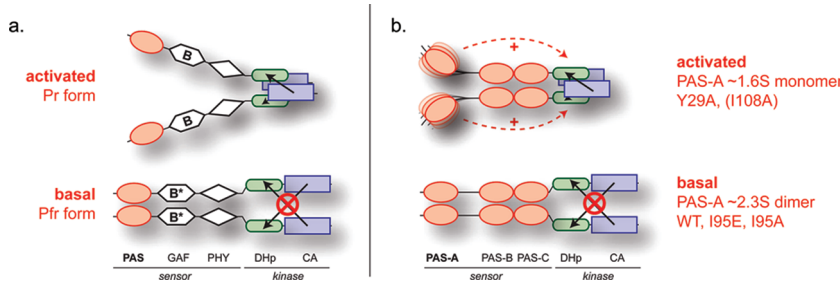

FIGURE 7: Model for bacteriophytochrome regulation and extension to *B. subtilis* KinA. (a) Model for bacteriophytochrome regulation, generated from limited proteolysis data and a proposal by Esteban et al. (*57*) and subsequently supported by small-angle X-ray scattering studies (*56*). In addition to PAS (red), DHp (green), and CA (purple) domains, bacteriophytochromes also contain a GAF domain (cyclic GMP/adenyl cyclase/FhiA domain (white hexagons); binds a bilin chromophore that isomerizes about the C15:C16 bond in response to illumination with red or far-red light (B, B*)) and a phytochrome-specific PHY domain (white diamonds). Reorientation of the sensory domains correlate with changes in the activity of the catalytic kinase domains. (b) Proposed changes in KinA as a function of the ability of the PAS-A domain to form stable dimers or participate in a monomer/dimer equilibrium with slow exchange within full-length KinA. Sedimentation coefficients of PAS-A constructs (wild type or containing various point mutations) are specified. Our model proposes that monomeric PAS-A is directly or indirectly capable of triggering changes in the arrangement of the DHp and CA domains (dashed arrows) that increase the efficiency of autophosphorylation but that dimeric forms cannot. The Y29A variant is shown to be significantly activated by several biophysical and biochemical criteria, while the I108A variant is activated less (designated with parentheses).

10–117) form a stable PAS domain fold with the ability to homodimerize as shown by X-ray crystallography, gel filtration chromatography, analytical ultracentrifugation, and NMR spectroscopy. This region contains the entire folded PAS-A domain, as shown by the poor chemical shift dispersion of signals from additional residues added to either end of the 10–117 construct. This idea is supported by limited proteolysis data from full-length KinA that indicate that PAS-A is tethered to the rest of the protein by a flexible, V8 protease-sensitive linker that is expected to be approximately 30 amino acids long (Figure 1a) (*17*). Our structural studies indicate that the dimer interface is formed by the surface of the central β-sheet that, in other PAS domains, participates in interactions with other proteins. Interestingly, this interface is used in different ways to generate the two dimeric forms we observed in the crystal. We note that a prior report has indicated that a similar domain fragment of KinA PAS-A (residues 1–139) was monomeric, as judged by gel filtration chromatography and native PAGE (*17*). On the basis of our own data showing that a comparable construct is dimeric (residues 1–138; Supporting Information, Figure S1), we suggest that this discrepancy stems from differences in sample preparation or the specific experimental conditions.

Turning to the function of PAS-A, we confirmed prior observations that the presence of this domain is integral to full KinA catalytic activity (*17*). We further established that changes in the solution dimerization state of the PAS-A domain correlate with changes of *in vitro* and *in vivo* kinase activity. These changes occur without perturbing the overall structure of the full-length KinA protein, which remained dimeric even when we introduced the Y29A point mutation that effectively disrupted the dimeric form of the isolated PAS-A domain (data not shown). Taken together, these data indicate that changes in the PAS-A domain alter kinase activity via an allosteric mechanism within a dimeric protein complex.

More generally, our data are consistent with observations from a wide range of sensor kinases that are regulated by PAS domains. Hidden Markov model-based domain searches of sequence databases (*51*) show that PAS domains are found in hundreds of soluble and membrane-bound putative sensor kinases. Several of these have been studied well enough to highlight the critical roles played by PAS domains in response to various stimuli, including oxygen (rhizobial FixL proteins (*52*)), small organic compounds (*Pseudomonas putida* TodS (*53*)), and quorum-sensing autoinducers (*Vibrio harveyi* LuxQ (*54*)). As with other kinds of sensory domains in this class of proteins, the details of the regulatory process have remained largely unclear. However, existing data collected on several systems indicate that changes in the dimerization behavior and/or spatial orientation of the PAS domains can alter the activity of the sensor by perturbing the arrangement of the catalytic CA and phosphoacceptor DHp domains. An example of this mechanism is provided by the membrane-integral LuxQ histidine kinase, part of the *Vibrio* quorum-sensing LuxP/Q two-component system. The LuxP protein, which is docked onto the PAS domains on the periplasmic surface of LuxQ, can bind a small organic autoinducer compound. When this binding event occurs, the dimeric LuxP/Q kinase complex is reoriented, thereby increasing the LuxQ catalytic activity located in the cytoplasm (*54, 55*).

Placing these observations in the context of the cytosolic KinA protein, one is led to mechanistic questions regarding how the distant PAS-A domains can influence the function of the KinA DHp and CA domains without having the topological constraints found in membrane-bound sensor kinases like LuxQ. Low-resolution structural data from two classes of soluble PAS-containing sensor kinases provide a useful framework for addressing these questions. One example is provided by studies of bacteriophytochromes, a class of light-dependent sensor kinases that switch between two different forms in response to red/far-red light illumination. This switch is achieved by a bilin chromophore bound within the bacteriophytochrome sensor domain (Figure 7a), forming a chromoprotein that undergoes photochemical conversion between red-absorbing (Pr) and far-red absorbing (Pfr) forms which have different catalytic activities. Small angle X-ray scattering studies of the active Pr form of a *Rps. palustris* bacteriophytochrome indicate that the dimeric bacteriophytochrome complex assumes an open Y shape, placing the two sensor domains far from each other, while phosphoacceptor DHp and catalytic CA domains from the

two monomers are close together, facilitating reciprocal phosphorylation (*56*). Complementary limited proteolysis and domain deletion studies of a cyanobacterial phytochrome indicate that photoconversion induces significant conformational changes in several sites within the sensor domain (*57*). These changes correlate with the dimerization state of the isolated sensor domain: this domain efficiently dimerizes in the inactive Pfr state, but is monomeric in the active Pr state. In summary, these data clearly suggest that differences in the interactions of sensor domains within a dimeric, soluble histidine kinase can be transmitted via an allosteric mechanism to control catalytic efficiency.

A possible mechanism for this linkage between sensor and catalytic domains can be based on biophysical studies of the *Thermotoga maritima* ThkA histidine kinase (*58*). Using a combination of small-angle X-ray scattering and low-resolution X-ray diffraction data collected on a PAS-DHp-CA construct of ThkA bound to the TrrA response regulator, Yamada and co-workers developed a low-resolution structural model that locates each ThkA PAS domain immediately adjacent to the DHp and CA domains of its own subunit. For KinA, such an arrangement could be facilitated by the ~40 residue flexible linker that attaches PAS-A to the rest of the protein, providing the freedom to potentially adopt an interaction to modulate KinA activity. Notably, KinA itself is regulated by two protein inhibitors that lower KinA enzymatic activity by directly interacting with the DHp/CA segment. One of these inhibitors, the 5 kDa Sda peptide, appears to work by binding onto the DHp domain (at a location similar to that observed for the PAS/DHp interaction of ThkA) and regulating kinase activity by an allosteric interaction (*59, 60*). The other inhibitor, the 27 kDa KipI protein, has been characterized as a noncompetitive inhibitor of KinA catalytic activity (*61*) that can directly inhibit a KinA DHp/CA fragment.

Integrating these data, we propose a model inspired by the bacteriophytochrome and ThkA results to link the catalytic activity of KinA to the PAS-A dimerization state or orientation (Figure 7b). This model assumes that an equilibrium exists between a basal and an activated form of KinA that differs in part by interactions assumed by the N-terminal PAS-A domain. Derivatives of PAS-A with significantly weakened homodimerization, most notably the Y29A and I108A variants, as shown by the lack of a dimeric 2.2 S species in sedimentation velocity data (Table 2), activate KinA. We suggest that this indicates that the PAS-A domains are liberated from PAS−PAS interactions, freeing them to interact with the DHp/CA region of the enzyme where we postulate that they will enhance autokinase activity. In contrast, mutants that still retain significant dimeric components of PAS-A, such as the I95E and I95A variants, will retain the basal form with lower kinase activity. For I95E, our data indicate that this mutation actually leads to significant kinase inhibition, both *in vitro* and *in vivo*, suggesting that this residue either plays a direct role in modulating kinase activity or alters some feature of the PAS-A dimer other than simply the monomer/dimer equilibrium.

It is important to emphasize that this model integrates biophysical studies of isolated PAS-A domains with functional data from the full-length KinA dimer, which will have two copies of PAS-A present at high local concentrations. We estimate that PAS-A domains are present at concentrations exceeding ~100 μM inside of the KinA dimer, assuming a 30 amino-acid linker between PAS-A and the rest of the protein. Of all of the KinA variants, only Y29A PAS-A had a dissociation constant clearly exceeding this value, and this mutant shows the strongest activation.

Given this high local concentration of PAS-A domains and the two different dimers observed in our PAS-A crystals, we speculate that these regulatory changes might be achieved not solely by altering the monomer/dimer equilibrium of the PAS-A domain but potentially also by interconversion between several different dimer configurations. We emphasize that our observation of multiple dimeric forms of PAS-A has been obtained by crystallographic studies of the isolated domain, and that the relevance of this finding remains to be established in the full-length protein. Analyses of both dimers using the web-based PISA service (*62*) indicate that dimer 2 should be stable in solution but fail to provide a conclusive statement about the potential stability of dimer 1. Structures of other PAS domains in dimeric complexes show that they use the same β-sheet interface as we observed for KinA PAS-A. Dimer orientations analogous to the two we have found can also be found among this collection of structures. For one of these domains, the PAS domain from the oxygen-sensing *B. japonicum* FixL sensor kinase, both dimers have been individually observed by using different conditions to generate crystals with different space groups (*63*), suggesting that the relative abundance of these two complexes may be environmentally dependent.

We close by emphasizing that we have changed KinA catalytic activity with artificial means (by either deleting domains or introducing point mutations into PAS-A), leaving open a number of questions about biological regulation. First, we emphasize that we believe that the 5-fold range of *in vitro* specific activities that we observed with a limited number of PAS-A point mutations (Table 2) does not represent the full physiological range of activity for this enzyme. Many histidine kinases show at least an order of magnitude change in activity upon physiological activation, which we reach only by comparing the specific activity of our most active KinA variant (Y29A) with an estimated value of the specific activity of ΔPAS-A based on data by Wang et al. (*17*). Regardless, our data still identify PAS-A as a potential regulatory site within this enzyme.

Second, reversible and timely regulation of KinA activity via PAS-A must occur by mechanisms other than the one we have described here. Notably, changes in the occupancy or configuration of small organic cofactors regulate the ability of other PAS domains to participate in intra or intermolecular protein interactions in other systems, including several sensor kinases. The binding of residues from chain A to chain D (Figure 2) suggests that PAS-A can perhaps accommodate ligand binding in regions similar to those where the sensory domain of FixL binds heme (*41*) or LOV-HK proteins bind FMN or FAD (*47*). Following a prior literature report of a potential candidate for this role (*64*), we have tested ATP for binding to PAS-A. However, we have not been able to demonstrate ATP binding using either fluorescence or NMR-based titration experiments at concentrations up to 20 mM Mg^{2+}-ATP, significantly higher than the 20 μM dissociation constant previously reported from photoaffinity labeling studies (*64*). While we cannot identify the source of this

discrepancy, we note that several additional ligand candidates have been suggested in the literature. These include small biological molecules (e.g., cis-saturated fatty acids (*65*)) whose levels might rise or decrease in response to the metabolic status of the cells. Alternatively, additional protein factors may also be involved. For example, the YheH protein, which putatively partners with YheI to form an ABC transporter, was identified as a KinA-interacting protein in a yeast two-hybrid study of *B. subtilis* protein/protein interactions. Overexpression of YheH/YheI significantly suppresses sporulation, suggesting that it may inhibit the KinA catalytic activity (*66*). These issues warrant additional study, providing further insight to address long-standing questions regarding the mechanism that links environmental conditions with the sporulation process itself.

ACKNOWLEDGMENT

The results shown in this report are derived from work performed at Argonne National Laboratory, Structural Biology Center at the Advanced Photon Source. Argonne is operated by UChicago Argonne, LLC, for the U.S. Department of Energy, Office of Biological and Environmental Research under contract DE-AC02-06CH11357.

SUPPORTING INFORMATION AVAILABLE

Gel filtration data for KinA(1–138), $^{15}N/^{1}H$ HSQC spectra of Y29A KinA(10–117) and additional data demonstrating GFP reporter assays of KinA function *in vivo*. This material is available free of charge via the Internet at http://pubs.acs.org.

REFERENCES

1. Stock, A. M., Robinson, V. L., and Goudreau, P. N. (2000) Two-component signal transduction. *Annu. Rev. Biochem. 69*, 183–215.
2. Falke, J. J., Bass, R. B., Butler, S. L., Chervitz, S. A., and Danielson, M. A. (1997) The two-component signaling pathway of bacterial chemotaxis: a molecular view of signal transduction by receptors, kinases, and adaptation enzymes. *Ann. Rev. Cell Dev. Biol. 13*, 457–512.
3. Gilles-Gonzalez, M. A., and Gonzalez, G. (2005) Heme-based sensors: defining characteristics, recent developments, and regulatory hypotheses. *J. Inorg. Biochem. 99*, 1–22.
4. Jacobs-Wagner, C. (2004) Regulatory proteins with a sense of direction: cell cycle signalling network in Caulobacter. *Mol. Microbiol. 51*, 7–13.
5. Swartz, T. E., Tseng, T.-S., Frederickson, M. A., Paris, G., Comerci, D. J., Rajashekara, G., Kim, J.-G., Mudgett, M. B., Splitter, G. A., Ugalde, R. A., Goldbaum, F. A., Briggs, W. R., and Bogomolni, R. A. (2007) Blue-light-activated histidine kinases: Two-component sensors in bacteria. *Science 317*, 1090–1093.
6. Galperin, M. Y., Nikolskaya, A. N., and Koonin, E. V. (2001) Novel domains of the prokaryotic two-component signal transduction systems. *FEMS Microbiol. Lett. 203*, 11–21.
7. Letunic, I., Copley, R. R., Pils, B., Pinkert, S., Schultz, J., and Bork, P. (2006) SMART 5: domains in the context of genomes and networks. *Nucleic Acids Res. 34*, D257–260.
8. Taylor, B. L., and Zhulin, I. B. (1999) PAS domains: internal sensors of oxygen, redox potential and light. *Microbiol. Mol. Biol. Rev. 63*, 479–506.
9. Erbel, P. J., Card, P. B., Karakuzu, O., Bruick, R. K., and Gardner, K. H. (2003) Structural basis for PAS domain heterodimerization in the basic helix–loop–helix-PAS transcription factor hypoxia-inducible factor. *Proc. Natl. Acad. Sci. U.S.A. 100*, 15504–15509.
10. Harper, S. M., Neil, L. C., and Gardner, K. H. (2003) Structural basis of a phototropin light switch. *Science 301*, 1541–1544.
11. Zoltowski, B. D., Schwerdtfeger, C., Widom, J., Loros, J. J., Bilwes, A. M., Dunlap, J. C., and Crane, B. R. (2007) Conformational switching in the fungal light sensor Vivid. *Science 316*, 1054–1057.
12. Burbulys, D., Trach, K. A., and Hoch, J. A. (1991) Initiation of sporulation in *B. subtilis* is controlled by a multicomponent phosphorelay. *Cell 64*, 545–552.
13. Perego, M., Cole, S. P., Burbulys, D., Trach, K., and Hoch, J. A. (1989) Characterization of the gene for a protein kinase which phosphorylates the sporulation-regulatory proteins Spo0A and Spo0F of *Bacillus subtilis*. *J. Bacteriol. 171*, 6187–6196.
14. Trach, K. A., and Hoch, J. A. (1993) Multisensory activation of the phosphorelay initiating sporulation in *Bacillus subtilis*: identification and sequence of the protein kinase of the alternate pathway. *Mol. Microbiol. 8*, 69–79.
15. Fujita, M., Gonzalez-Pastor, J. E., and Losick, R. (2005) High- and low-threshold genes in the Spo0A regulon of *Bacillus subtilis*. *J. Bacteriol. 187*, 1357–1368.
16. Varughese, K. I., Zhao, H., Veldore, V. H., and Zapf, J. (2007) Sporulation phosphorelay proteins and their complexes: crystallographic characterization. *Methods Enzymol. 422*, 102–122.
17. Wang, L., Fabret, C., Kanamaru, K., Stephenson, K., Dartois, V., Perego, M., and Hoch, J. A. (2001) Dissection of the functional and structural domains of phosphorelay histidine kinase A of *Bacillus subtilis*. *J. Bacteriol. 183*, 2795–2802.
18. Otwinowski, Z., and Minor, W. (1997) Processing of X-ray diffraction data collected in oscillation mode. *Meth. Enz. 276*, 307–326.
19. Schneider, T. R., and Sheldrick, G. M. (2002) Substructure solution with SHELXD. *Acta Crystallogr. 58*, 1772–1779.
20. Otwinowski, Z. (1991) In *Isomorphous Replacement and Anomalous Scattering. Proceedings of CCP4 Study Weekend* (Wolf, W., Evans, P. R., and Leslie, A. G. W., Eds.), pp 80–86, Daresbury Laboratory, Warrington, England.
21. Collaborative Computational Project, N. (1994) The CCP4 suite: programs for protein crystallography. *Acta Crystallogr., Sect. D 50*, 760–763.
22. Morris, R. J., Zwart, P. H., Cohen, S., Fernandez, F. J., Kakaris, M., Kirillova, O., Vonrhein, C., Perrakis, A., and Lamzin, V. S. (2004) Breaking good resolutions with ARP/wARP. *J. Synchrotron Radiat. 11*, 56–59.
23. Jones, T. A., Zou, J. Y., and Cowan, S. W. (1991) Improved methods for building protein models in electron density maps and the location of errors in these models. *Acta Crystallogr., Sect. A 47*, 110–119.
24. Brunger, A. T., Adams, P. D., Clore, G. M., DeLano, W. L., Gros, P., Grosse-Kunstleve, R. W., Jiang, J. S., Kuszewski, J., Nilges, M., Pannu, N. S., Read, R. J., Rice, L. M., Simonson, T., and Warren, G. L. (1998) Crystallography & NMR system: A new software suite for macromolecular structure determination. *Acta Crystallogr. 54*, 905–921.
25. Murshudov, G. N., Vagin, A. A., Lebedev, A., Wilson, K. S., and Dodson, E. J. (1999) Efficient anisotropic refinement of macromolecular structures using FFT. *Acta Crystallogr., Sect. D 55*, 247–255.
26. Davis, I. W., Murray, L. W., Richardson, J. S., and Richardson, D. C. (2004) MOLPROBITY: structure validation and all-atom contact analysis for nucleic acids and their complexes. *Nucleic Acids Res. 32*, W615–619.
27. Baker, N. A., Sept, D., Joseph, S., Holst, M. J., and McCammon, J. A. (2001) Electrostatics of nanosystems: application to microtubules and the ribosome. *Proc. Natl. Acad. Sci. U.S.A. 98*, 10037–10041.
28. Lee, B., and Richards, F. M. (1971) The interpretation of protein structures: estimation of static accessibility. *J. Mol. Biol. 55*, 379–400.
29. Shatsky, M., Nussinov, R., and Wolfson, H. J. (2004) A method for simultaneous alignment of multiple protein structures. *Proteins 56*, 143–156.
30. Yamazaki, T., Lee, W., Arrowsmith, C. H., Muhandiram, D. R., and Kay, L. E. (1994) A suite of triple resonance NMR experiments for the backbone assignment of ^{15}N, ^{13}C, ^{2}H labeled proteins with high sensitivity. *J. Am. Chem. Soc. 116*, 11655–11666.
31. Sattler, M., Schleucher, J., and Griesinger, C. (1999) Heteronuclear multidimensional NMR experiments for the structure determination of proteins in solution employing pulsed field gradients. *Prog. Nucl. Magn. Reson. Spectrosc. 34*, 93–158.
32. Pascal, S. M., Muhandiram, D. R., Yamazaki, T., Forman-Kay, J. D., and Kay, L. E. (1994) Simultaneous acquisition of ^{15}N- and ^{13}C-edited NOE spectra of proteins dissolved in H_2O. *J. Magn. Reson. B 103*, 197–201.

33. Kay, L. E., Keifer, P., and Saarinen, T. (1992) Pure absorption gradient-enhanced heteronuclear single quantum correlation spectroscopy with improved sensitivity. *J. Am. Chem. Soc. 114*, 10663–10665.
34. Delaglio, F., Grzesiek, S., Vuister, G. W., Zhu, G., Pfeifer, J., and Bax, A. (1995) NMRPipe: a multidimensional spectral processing system based on UNIX pipes. *J. Biomol. NMR 6*, 277–293.
35. Johnson, B. A. (2004) Using NMRView to visualize and analyze the NMR spectra of macromolecules. *Methods Mol. Biol. 278*, 313–352.
36. Schuck, P. (2003) On the analysis of protein self-association by sedimentation velocity analytical ultracentrifugation. *Anal. Biochem. 320*, 104–124.
37. Sheffield, P., Garrard, S., and Derewenda, Z. (1999) Overcoming expression and purification problems of RhoGDI using a family of "parallel" expression vectors. *Protein Expression Purif. 15*, 34–39.
38. Veening, J. W., Kuipers, O. P., Brul, S., Hellingwerf, K. J., and Kort, R. (2006) Effects of phosphorelay perturbations on architecture, sporulation, and spore resistance in biofilms of *Bacillus subtilis*. *J. Bacteriol. 188*, 3099–3109.
39. Fujita, M., and Losick, R. (2005) Evidence that entry into sporulation in *Bacillus subtilis* is governed by a gradual increase in the level and activity of the master regulator Spo0A. *Genes Dev. 19*, 2236–2244.
40. Hendrickson, W. A., Horton, J. R., Murthy, H. M., Pahler, A., and Smith, J. L. (1989) Multiwavelength anomalous diffraction as a direct phasing vehicle in macromolecular crystallography. *Basic Life Sci. 51*, 317–324.
41. Gong, W., Hao, B., Mansy, S. S., Gonzalez, G., Gilles-Gonzalez, M. A., and Chan, M. K. (1998) Structure of a biological oxygen sensor: a new mechanism for heme-driven signal transduction. *Proc. Natl. Acad. Sci. U.S.A. 95*, 15177–15182.
42. Borgstahl, G. E., Williams, D. R., and Getzoff, E. D. (1995) 1.4 A structure of photoactive yellow protein, a cytosolic photoreceptor: unusual fold, active site, and chromophore. *Biochemistry 34*, 6278–6287.
43. Zoltowski, B. D., Schwerdtfeger, C., Widom, J., Loros, J. J., Bilwes, A. M., Dunlap, J. C., and Crane, B. R. (2007) Conformational switching in the fungal light sensor vivid. *Science 316*, 1054–1057.
44. Gong, W., Hao, B., Mansy, S. S., Gonzalez, G., Gilles-Gonzalez, M. A., and Chan, M. K. (1998) Structure of a biological oxygen sensor: a new mechanism for heme-driven signal transduction. *Proc. Natl. Acad. Sci. U.S.A. 95*, 15177–15182.
45. Chen, J., Zou, A., Splawski, I., Keating, M. T., and Sanguinetti, M. C. (1999) Long QT syndrome-associated mutations in the Per-Arnt-Sim (PAS) domain of HERG potassium channels accelerate channel deactivation. *J. Biol. Chem. 274*, 10113–10118.
46. Card, P. B., Erbel, P. J. A., and Gardner, K. H. (2005) Structural basis of ARNT PAS-B dimerization: Use of a common beta-sheet interface for hetero- and homodimerization. *J. Mol. Biol. 353*, 664–677.
47. Crosson, S., and Moffat, K. (2001) Structure of a flavin-binding plant photoreceptor domain: Insights into light-mediated signal transduction. *Proc. Natl. Acad. Sci. U.S.A. 98*, 2995–3000.
48. Yildiz, 951 > O., Doi, M., Yujnovsky, I., Cardone, L., Berndt, A., Hennig, S., Schulze, S., Urbanke, C., Sassone-Corse, P., and Wolf, E. (2005) Crystal structure and interactions of the PAS repeat region of the Drosophila clock protein PERIOD. *Mol. Cell 17*, 69–82.
49. Garcia De La Torre, J., Huertas, M. L., and Carrasco, B. (2000) Calculation of hydrodynamic properties of globular proteins from their atomic-level structure. *Biophys. J. 78*, 719–730.
50. Wagner, G. (1997) An account of NMR in structural biology. *Nat. Struct. Biol. 4*, 841.
51. Finn, R. D., Mistry, J., Schuster-Bockler, B., Griffiths-Jones, S., Hollich, V., Lassmann, T., Moxon, S., Marshall, M., Khanna, A., Durbin, R., Eddy, S. R., Sonnhammer, E. L., and Bateman, A. (2006) Pfam: clans, web tools and services. *Nucleic Acids Res. 34*, D247–251.
52. Gilles-Gonzalez, M. A., and Gonzalez, G. (1993) Regulation of the kinase activity of heme protein FixL from the two-component system FixL/FixJ of *Rhizobium meliloti*. *J. Biol. Chem. 268*, 16293–16297.
53. Busch, A., Lacal, J., Martos, A., Ramos, J. L., and Krell, T. (2007) Bacterial sensor kinase TodS interacts with agonistic and antagonistic signals. *Proc. Natl. Acad. Sci. U.S.A. 104*, 13774–13779.
54. Neiditch, M. B., Federle, M. J., Pompeani, A. J., Kelly, R. C., Swem, D. L., Jeffrey, P. D., Bassler, B. L., and Hughson, F. M. (2006) Ligand-induced asymmetry in histidine sensor kinase complex regulates quorum sensing. *Cell 126*, 1095–1108.
55. Neiditch, M. B., Federle, M. J., Miller, S. T., Bassler, B. L., and Hughson, F. M. (2005) Regulation of LuxPQ receptor activity by the quorum-sensing signal autoinducer-2. *Mol. Cell 18*, 507–518.
56. Evans, K., Grossmann, J. G., Fordham-Skelton, A. P., and Papiz, M. Z. (2006) Small-angle X-ray scattering reveals the solution structure of a bacteriophytochrome in the catalytically active Pr state. *J. Mol. Biol. 364*, 655–666.
57. Esteban, B., Carrascal, M., Abian, J., and Lamparter, T. (2005) Light-induced conformational changes of cyanobacterial phytochrome Cph1 probed by limited proteolysis and autophosphorylation. *Biochemistry 44*, 450–461.
58. Yamada, S., Akiyama, S., Sugimoto, H., Kumita, H., Ito, K., Fujisawa, T., Nakamura, H., and Shiro, Y. (2006) The signaling pathway in histidine kinase and the response regulator complex revealed by X-ray crystallography and solution scattering. *J. Mol. Biol. 362*, 123–139.
59. Rowland, S. L., Burkholder, W. F., Cunningham, K. A., Maciejewski, M. W., Grossman, A. D., and King, G. F. (2004) Structure and mechanism of action of Sda, an inhibitor of the histidine kinases that regulate initiation of sporulation in *Bacillus subtilis*. *Mol. Cell 13*, 689–701.
60. Whitten, A. E., Jacques, D. A., Hammouda, B., Hanley, T., King, G. F., Guss, J. M., Trewhella, J., and Langley, D. B. (2007) The structure of the KinA-Sda complex suggests an allosteric mechanism of histidine kinase inhibition. *J. Mol. Biol. 368*, 407–420.
61. Wang, L., Grau, R., Perego, M., and Hoch, J. A. (1997) A novel histidine kinase inhibitor regulating development in *Bacillus subtilis*. *Genes Dev. 11*, 2569–2579.
62. Krissinel, E., and Henrick, K. (2007) Inference of macromolecular assemblies from crystalline state. *J. Mol. Biol. 372*, 774–797.
63. Zhong, X., Hao, B., and Chan, M. K. (2003) Structure of the PAS Fold and Signal Transduction Mechanisms, in *PAS Proteins: Regulators and Sensors of Development and Physiology* (Crews, S. T., Ed.), pp 1–16, Kluwer, Dordrecht, The Netherlands.
64. Stephenson, K., and Hoch, J. A. (2001) PAS-A domain of phosphorelay sensor kinase A: a catalytic ATP-binding domain involved in the initiation of development in *Bacillus subtilis*. *Proc. Natl. Acad. Sci. U.S.A. 98*, 15251–15256.
65. Strauch, M. A., de Mendoza, D., and Hoch, J. A. (1992) cis-unsaturated fatty acids specifically inhibit a signal-transducing protein kinase required for initiation of sporulation in *Bacillus subtilis*. *Mol. Microbiol. 6*, 2909–2917.
66. Fukushima, S., Yoshimura, M., Chibazakura, T., Sato, T., and Yoshikawa, H. (2006) The putative ABC transporter YheH/YheI is involved in the signalling pathway that activates KinA during sporulation initiation. *FEMS Microbiol. Lett. 256*, 90–97.

BI7021156